Proceedings of the 2003 IEEE International Frequency Control Symposium and PDA Exhibition
Jointly with the 17th European Frequency and Time Forum

INTEGRATED ELECTROMAGNETIC–VIBROACOUSTIC HIGH-FIDELITY MODELING, SIMULATION AND OPTIMIZATION OF MICROELECTROMECHANICAL MOTION DEVICES

Sergey Edward Lyshevski
Department of Electrical Engineering, Rochester Institute of Technology, Rochester, New York 14623-5603, USA
E-mail: seleee@rit.edu; Web: www.rit.edu/~seleee

Abstract – **This paper addresses and solves complex electromagnetic–vibroacoustic problems for rotational microscale electromechanical motion devices (MEMDs). The results reported enable one to straightforwardly and explicitly apply fundamental concepts developed to utilize the full potential of MEMDs attaining optimal overall performance. The studied MEMDs are the electromagnetic-based rotational devices. Correspondingly, coherent analysis and design must be performed. We report novel paradigms integrating complex electromagnetic, electromechanical and vibro-acoustic nonlinear phenomena and effects. It is demonstrated that there is a need to design and optimize electromagnetic-electromechanical systems as well as to device novel MEMDs topologies and architectures.**

Keywords **– electromagnetics, microelectromechanical motion devices, modeling, optimization, vibroacoustics**

I. INTRODUCTION

To guarantee the optimal performance, there is the need to depart form conventional analysis and design concepts that are based on assumptions and simplifications that not valid. In particular, many analysis and design concepts are based on lamped-parameter mathematical models, steady-state analysis, linearization concepts, etc. Significant deficiencies of these approaches lead to incomprehensive design. Correspondingly, undesirable effects result, e.g., vibration, noise, overheating, wearing, etc. To compensate the undesirable effects, which can be due to inadequate design, different concepts have been proposed in [1-3]. E.g., passive and active vibration attenuation, noise cancellation, etc. However, high efficiency, robustness, low noise and vibration, durability, reliability and other highly desirable characteristics of MEMDs can be achieved trough optimal design. This coherent design should integrate integrated electromagnetic – vibroacoustic high-fidelity modeling, heterogeneous simulation and optimization. For example, through these well-defined logical sequential steps, one can eliminate torque ripple, optimize electromagnetic system, minimize electromagnetic interference, eliminate vibrations, attenuate noise, etc.

This paper is concentrated on development of integrated modeling, analysis and optimization methods to coherently assess and control electromagnetic, electro-mechanical and vibroacoustic phenomena in mini- and microscale transducers. A high-fidelity modeling paradigm reported allows one to achieve the highest degree of confidence in simulation and design. It is illustrated that it is necessary not only to attain the analysis with accurate performance prediction and assessment, but also devise and apply novel electromagnetic-mechanical optimization concepts and vibroacoustic reduction methods. Therefore, we study the integrated electromagnetics – electromechanics – vibroacoustics, as well as devise and analyze novel vibration and noise attenuation concepts.

In this paper, radial and axial topology MEMDs are examined. It is shown that there is possible to optimize electromagnetic-electromechanical systems and reduce noise and vibration that have low-, medium- and high-frequency spectra. In contrast, simplifications and assumptions, that could be made to simplify electromagnetic-mechanical analysis, in general, do not allow one to attain accuracy. We formulate and solve the computationally tractable integrated electromagnetic–mechanical–vibroacoustic problem. The fundamental, applied, numerical, and experimental results documented show that conventional MEMDs have high level of noise and vibration at medium and high frequency. These medium and high frequency vibrations needed to be reduced. The alternative results have been reported in the literature only for low frequency. Furthermore, high-fidelity mathematical models have not been developed and applied. In this paper, mathematical models for electromagnetic and electromechanical systems are validated performing experiments. Based upon high-fidelity modeling, we perform optimization and control. The experimental results illustrate that high performance is achieved for different radial and axial topology MEMDs.

II. PERMANENT-MAGNET MICROELECTROMECHNAICAL MOTION DEVICES

Distinct electrostatic and electromagnetic MEMDs can be designed and fabricated using the surface micromachining technology [4]. However, all high-performance, high power and torque densities MEMDs are electromagnetic, and these MEMDs use permanent micromagnets. Therefore, the issues of fabrication and analysis of micromagnets are of great interest.

Different *soft* and *hard* micromagnets can be fabricated using surface micromachining. E.g., Ni, Fe, Co, NiFe, and other magnets can be made. In general, four classes of high-performance magnets have been commonly used in electromechanical motion devices, e.g., neodymium iron boron ($Nd_2Fe_{14}B$), samarium cobalt (usually Sm_1Co_5 and

0-7803-7688-9/03/$17.00 © 2003 IEEE

Sm_2Co_{17}), ceramic (ferrite) and alnico (AlNiCo). The term *soft* is used to describe those magnets that have high saturation magnetization and a low coercivity (narrow *BH* curve). Another property of these micromagnets is their low magnetostriction. The *soft* micromagnets have been widely used in magnetic recording heads, and NiFe thin films with the desired properties have been fabricated [4]. *Hard* magnets have wide *BH* curves (high coercivity), and, therefore, high-energy storage capacity. These micromagnets should be used in MEMDs in order to attain high force, torque and power densities. Unfortunately, limited progress has been made in the fabrication of *hard* micromagnets. Most *hard* magnets are fabricated using the following processes: (1) metallurgical – sintering (creating a solid but porous material from a powder), pressure bonding, injection molding, casting, and extruding; (2) vacuum – evaporation, sputtering, molecular beam epitaxy (MBE), and chemical vapor deposition (CVD); (3) electrochemical – electroless deposition and electroplating. Many of these processes are incompatible with ICs. Electroplating has been used to fabricate the Co-based *hard* micromagnets. The saturation magnetization decreases with increases in the amount of nonmagnetic alloy adding P, As, Sb, Bi, W, Cr, Mo, Pd, Pt, Ni, Fe, Cu, Mn, etc. For example, CoPt and FePt thin films have high coercivities. The Co-based micromagnets have been usually deposited using MBE and sputtering techniques. These processes require high temperatures (up to 700°C) during annealing. Neodymium iron boron micromagnets can be micro-fabricated using injection molding and pressure bonding methods. Both CoPt and NdFeB *hard* magnets can be vacuum deposited. However, high temperatures (of either the material or the substrate) need to be achieved to anneal the final deposition (if it is not annealed, the material acts as a *soft* magnet).

The energy density is given as the area enclosed by the *BH* curve, e.g., $w_m = \frac{1}{2}\mathbf{B}\cdot\mathbf{H}$. When micromagnets are used in MEMDs, the demagnetization curve (second quadrant of the *BH* curve) is studied. The operating point is denoted by H_d and B_d. Given an air gap through which the magnetic flux exists in MEMDs, according to Ampere's law, we have

$$H_d l_m = H_{ag} l_{ag},$$

where l_m is the length of the magnet; l_{ag} is the length of the air gap parallel to the flux lines; H_{ag} is the magnetic field intensity in the air gap.

The cross-sectional area of a magnet required to produce a specific flux density in the air gap is

$$A_m = \frac{B_{ag} A_{ag}}{B_d}$$

where A_{ag} is the area of the air gap; B_{ag} is the flux density in the gap.

The flux linkages due to the magnet in the air gap are $\psi = N\phi = NB_{ag}A_{ag}$, and the co-energy is given by [4]

$$W = \int_{\psi} i\cdot d\psi = \int_{i} \psi\cdot di\cdot$$

In a lossless system [4], an informative energy equation for the air gap is

$$Vol_{ag} B_{ag} H_{ag} = A_{ag} l_{ag} \frac{A_m l_m B_d H_d}{A_{ag} l_{ag}} = A_m l_m B_d H_d = \psi i\cdot$$

The flux density at position $\boldsymbol{x}$ can be derived, and high-fidelity mathematical models are found [4]. In one-dimensional case for cylindrical micromagnets (length l_m and radius r) that have *near-linear* demagnetization curves, the flux density at a distance x is approximated as

$$B = \frac{B_r}{2}\left(\frac{l_m + x}{\sqrt{r^2 + (l_m + x)^2}} - \frac{x}{\sqrt{r^2 + x^2}}\right)\cdot$$

III. High-Fidelity Modeling of Electromagnetic-Vibroacoustic Phenomena in MEMDs

To perform data-intensive analysis, optimal design, performance assessment and optimization of MEMDs, high-fidelity mathematical models are needed to describe the dynamics of complex electromagnetic, electro-mechanical, and vibroacoustic phenomena. We augment electromagnetic-mechanical-vibroacoustic models to study complex effects and perform optimization with ultimate objectives to guarantee efficiency, robustness, durability and stealth. Vibration and noise result due to very complex electromagnetic-electromechanical-vibroacoustic phenomena. Correspondingly, the simplifications are not valid. Therefore, we will develop high-fidelity mathematical models.

3.1. Nonlinear Electromagnetics

Electromagnetic fields modeling is performed applying Maxwell's equations and tensor calculus [4]. The following partial differential equations describe time-varying electromagnetic fields in MEMDs

$$\nabla\times\mathbf{E} = -\mu\frac{\partial\mathbf{H}}{\partial t},\ \nabla\times\mathbf{H} = \sigma\mathbf{E} + \mathbf{J},$$

$$\nabla\cdot\mathbf{E} = \frac{\rho_v}{\varepsilon},\ \nabla\cdot\mathbf{H} = 0, \qquad (1)$$

where **E** and **H** are the electric and magnetic field intensities; **J** is the current density; ε, μ and σ are the permittivity, permeability and conductivity; ρ_v is the volume charge density.

The Lorenz force, which relates the electromagnetic and mechanical phenomena, is

$$\mathbf{F} = \rho_v(\mathbf{E} + \mathbf{v}\times\mathbf{B}) = \rho_v\mathbf{E} + \mathbf{J}\times\mathbf{B}.$$

The electromagnetic force is found applying the Maxwell stress tensor method. This concept employs a volume integral to obtain the stored energy, and

$$\mathbf{F}=\int_v(\rho_v\mathbf{E}+\mathbf{J}\times\mathbf{B})dv=\frac{1}{\mu}\oint_s\vec{\vec{T}}_{\alpha\beta}\cdot d\mathbf{s},$$

where the electromagnetic stress energy tensor is

$$\vec{\vec{T}}_{\alpha\beta}=\begin{bmatrix}0 & \vec{E}_x & \vec{E}_y & \vec{E}_z\\ -\vec{E}_x & 0 & \vec{B}_z & -\vec{B}_y\\ -\vec{E}_y & -\vec{B}_z & 0 & \vec{B}_x\\ -\vec{E}_z & \vec{B}_y & -\vec{B}_x & 0\end{bmatrix}.$$

Thus, the electromagnetic torque developed by MEMDs is found using the electromagnetic field variables. The electromagnetic stress tensor is

$$T_s=T_s^E+T_s^M$$
$$=\begin{bmatrix}E_1D_1-\frac{1}{2}E_jD_j & E_1D_2 & E_1D_3\\ E_2D_1 & E_2D_2-\frac{1}{2}E_jD_j & E_2D_3\\ E_3D_1 & E_3D_2 & E_3D_3-\frac{1}{2}E_jD_j\end{bmatrix}$$
$$+\begin{bmatrix}B_1H_1-\frac{1}{2}B_jH_j & B_1H_2 & B_1H_3\\ B_2H_1 & B_2H_2-\frac{1}{2}B_jH_j & B_2H_3\\ B_3H_1 & B_3H_2 & B_3H_3-\frac{1}{2}B_jH_j\end{bmatrix}.$$

The expression for the airgap flux density $\mathbf{B}_{ag}$ must be found to perform torque, *back emf*, vibration and noise analysis. For two regions (airgap *ag* and permanent magnets *pm*), we have

$$\mathbf{B}_{ag}=\mu_0\mathbf{H}_{ag},$$
$$\mathbf{B}_{pm}=\mu_0\mathbf{H}_{pm}+\mathbf{J}=\mu_0(\mu_r\mathbf{H}_{pm}+\mathbf{M}),$$

where $\mathbf{M}$ is the residual magnetization vector, and for radially magnetized magnets $M=B_r/\mu$; B_r is the remanence; μ_r is the relative recoil permeability.

The negative gradient of the scalar magnetic potential V gives the magnetic field intensity,

$$\mathbf{H}=-\nabla V.$$

The scalar magnetic potential satisfies the Laplace equation in free and homogeneous media (with zero current density, e.g., $\mathbf{J}$=0). For radial topology MEMDs we have

$$H_r=-\frac{\partial V}{\partial r},$$
$$H_\theta=-\frac{1}{r}\frac{\partial V}{\partial\theta},$$
$$\frac{\partial^2V_{ag}}{\partial r^2}+\frac{1}{r}\frac{\partial V_{ag}}{\partial r}+\frac{1}{r^2}\frac{\partial^2V_{ag}}{\partial\theta^2}=0,$$
$$\frac{\partial^2V_{pm}}{\partial r^2}+\frac{1}{r}\frac{\partial V_{pm}}{\partial r}+\frac{1}{r^2}\frac{\partial^2V_{pm}}{\partial\theta^2}=\frac{1}{r\mu_r}M_r.$$

Assuming uniform magnetization, one obtains

$$M_r=\frac{2}{\mu_0}B_r\sum_{i=1,3,5,\ldots}^{\infty}\frac{\sin(\frac{1}{2}i\pi)}{\frac{1}{2}i\pi}\cos(ip\theta)\ \text{ and }\ M_\theta=0.$$

Using the boundary conditions, the general solution for the airgap flux density B_{ag} is found using the Fourier series solution.

For axial topology MEMDs, the cylindrical coordinate system is used. We have

$$\nabla\cdot\mathbf{M}=\frac{1}{r}\frac{\partial(rM_r)}{\partial r}+\frac{1}{r}\frac{\partial M_\phi}{\partial r}+\frac{\partial M_z}{\partial z}.$$

Solving the partial differential equation

$$\frac{1+\chi_t}{r}\frac{\partial}{\partial r}\left(r\frac{\partial V}{\partial r}\right)+\frac{1+\chi_t}{r^2}\frac{\partial^2V}{\partial\phi^2}+(1+\chi)\frac{\partial^2V_{ag}}{\partial z^2}=\nabla\cdot\mathbf{M},$$

the three-dimensional airgap flux density is found as

$$B_{agz}(r,\phi,z)=\frac{\mu_0M_0}{1+\chi}\sum_{i=1}^{\infty}a_i\frac{\sinh\frac{\nu_i\varepsilon h_r}{r}}{\sinh\frac{\nu_i\varepsilon(h_r+g_{ag})}{r}}\cosh\frac{\nu_i\varepsilon z}{r}\sin\nu_i\phi,$$

where χ and χ_t are the reversible susceptibility along the easy and transverse magnetization axes; a_i is the harmonic amplitude coefficient, and for the trapezoidal-wave magnetization, $a_i=\frac{4\sin(2i-1)}{\pi(2i-1)^2}$; $h_r\le z\le g_{ag}+h_r$, h_r is the rotor thickness.

One-dimensional airgap flux density is found to be

$$B_{agz}(\phi)=\frac{\mu_0M_0h_r}{(1+\chi)(h_r+g_{ag})}\sum_{i=1}^{\infty}a_i\sin\nu_i\phi,$$

and the maximum flux density in the airgap is

$$B_{\max z}=\frac{\mu_0M_0h_r}{(1+\chi)(h_r+g_{ag})}\sum_{i=1}^{\infty}a_i(-1)^{i+1}.$$

Using the derived equations for the airgap flux density and *emf*, one finds three-dimensional electromagnetic forces and torques to coherently study torque production, vibration, noise and other complex phenomena in MEMDs.

3.2. Multimode Vibration Analysis

Let us demonstrate the viable application of the Lagrangian mechanics and Fourier analysis for the complex geometrically/structurally interfered vibroacoustic systems in MEMDs that exhibit low-, medium- and high-frequency vibrations due to short-, middle- and long-wavelength deformations. Our goal is to develop the *multimode vibration* analysis methodology.

The vibroacoustic behavior of MEMDs contains smooth function modes of different subsystems, e.g., shaft, rotor, shell, acoustic cavity, bearing, etc. Using the basis (admissible) functions $\phi(\mathbf{x})$ and generalized system coordinates $\mathbf{q}$, for N subsystems, the displacement modes $\mathbf{r}=\begin{bmatrix}r_1\\ r_2\\ r_3\end{bmatrix}$ at the general location $\mathbf{x}=\begin{bmatrix}x_1\\ x_2\\ x_3\end{bmatrix}$ are given as

$$\mathbf{r}(t,\mathbf{x})=\sum_{k=1}^{\infty}q_k(t)\phi_k(\mathbf{x}).$$

Using the Lagrangian mechanics, one finds

$$M\ddot{\mathbf{q}}+C\dot{\mathbf{q}}+K\mathbf{q}=\mathbf{Q},$$

where $\mathbf{q}$ and $\mathbf{Q}$ are the generalized coordinates and forces, $Q_i(t)=\sum_{n=1}^{N}\int_V Q_{Ln}(t,\mathbf{x})^T\phi_i(\mathbf{x})d\mathbf{x}$; $Q_{Ln}(t,\mathbf{x})$ is the time-varying

distributed loads acting on the *n*th subsystem; *M*, *C* and *K* are the mass, damping and stiffness matrices, and the *ij* entries of the *M* and *K* matrices are given as

$$m_{ij} = \sum_{n=1}^{N} \int_V \rho_n(\mathbf{x}) \phi_i^T(\mathbf{x}) \phi_j^T(\mathbf{x}) d\mathbf{x} \text{ and}$$

$$k_{ij} = \sum_{n=1}^{N} \int_V \left(d_n(\mathbf{x}) \phi_i(\mathbf{x})\right)^T D_n d_n(\mathbf{x}) \phi_j(\mathbf{x}) d\mathbf{x};$$

$\rho_n(\mathbf{x})$ is the volume density for the *n*th subsystem; $d_n(\mathbf{x})$ is the differential operator matrix which acts of the system displacements $\mathbf{r}$ to produce the strain $\boldsymbol{\varepsilon}_n$, $\boldsymbol{\varepsilon}_n = d_n(\mathbf{x})\mathbf{r}$; D_n is the constitutive matrix which relates the stress $\boldsymbol{\sigma}_n$ and strain $\boldsymbol{\varepsilon}_n$ vectors, $\boldsymbol{\sigma}_n = D_n \boldsymbol{\varepsilon}_n$ (in three-dimensional case, stress and strain have six components, e.g., three direct terms and three shear terms).

Using the Fourier transform, one finds the solution of the Lagrange equation in the frequency domain. In particular, we have

$$\left[-\omega^2 M + j\omega C + K\right]\mathbf{q} = \mathbf{Q} \text{ or } D\mathbf{q} = \mathbf{Q},$$

where ω is the frequency; *D* is the dynamic stiffness matrix.

The expression for the stiffness matrix is

$$D = -\omega^2 M + j\omega C + K.$$

In the rotational motion devices, there are bending, torsional and axial elastic waves. The bending waves have much shorter wavelength compared with the axial and torsional waves. Thus, we have the short, medium and long wavelength deformations and modes that needed to be examined. The short, medium and long basis functions $\phi_S(\mathbf{x})$, $\phi_M(\mathbf{x})$ and $\phi_L(\mathbf{x})$ are used to find the displacement modes

$$\mathbf{r}(t,\mathbf{x}) = \sum_{k=1}^{\infty} q_{Sk}(t)\phi_{Sk}(\mathbf{x}) + \sum_{k=1}^{\infty} q_{Mk}(t)\phi_{Mk}(\mathbf{x}) + \sum_{k=1}^{\infty} q_{Lk}(t)\phi_{Lk}(\mathbf{x})$$

Making note of

$$D\mathbf{q} = \mathbf{Q},$$

we have

$$\begin{bmatrix} D_{SS} & D_{SM} & D_{SL} \\ D_{SM}^T & D_{MM} & D_{ML} \\ D_{SL}^T & D_{ML}^T & D_{LL} \end{bmatrix} \begin{bmatrix} \mathbf{q}_S \\ \mathbf{q}_M \\ \mathbf{q}_L \end{bmatrix} = \begin{bmatrix} \mathbf{Q}_S \\ \mathbf{Q}_M \\ \mathbf{Q}_L \end{bmatrix},$$

where $\mathbf{q}_S$, $\mathbf{q}_M$ and $\mathbf{q}_L$ are the generalized coordinates characterizing the short, medium and long wavelength; D_{SS}, D_{MM} and D_{LL} are the diagonal matrices, and their entries are found as $d_{ii} = \omega_i^2(1 + j\mu_i) - \omega^2$; ω_i and μ_i are the natural frequency and loss factor associated with the *i*th mode; D_{SM}, D_{SL} and D_{ML} are partition matrices which model the coupling effect.

To find D_{SM}, D_{SL} and D_{ML}, *M*, *C* and *K* matrices must be appropriately partitioned. The approximation can be performed. For example, using the dominant modes assuming that the damping can be neglected, one has

$$D_{SM} \approx -\omega^2 M_{SM},\ D_{SL} \approx -\omega^2 M_{SL} \text{ and } D_{ML} \approx -\omega^2 M_{ML},$$

where M_{SM}, M_{SL} and M_{ML} are matrices obtained by partitioning the matrix *M*.

Illustrative Example.

To illustrate the viability and efficiency of the proposed concept, for MEMDs, the rotor axial displacement modes are modeled as

$$\mathbf{r}(t,\mathbf{x}) = q_1(t)\left(1 - \frac{x}{l}\right) + q_2(t)\frac{x}{l} + \sqrt{\frac{2}{\rho A l}} \sum_{k=1}^{\infty} q_{k+2}(t) \sin\left(k\pi \frac{x}{l}\right),$$

where q_1 and q_2 are the nodal displacements at two ends; q_{k+2} is the amplitude of the *k*+2 function; *l* and *A* are the length and cross-sectional area.

The nonzero entries of the upper triangle of the mass and stiffness matrices are

$$m_{11} = m_{22} = \tfrac{1}{3}\rho A l,\ m_{12} = \tfrac{1}{6}\rho A l,\ m_{1,k+2} = \frac{\sqrt{2\rho A l}}{k\pi},$$

$$m_{2,k+2} = -(-1)^k \frac{\sqrt{2\rho A l}}{k\pi},\ m_{k+2,k+2} = 1,\ k_{11} = k_{22} = \frac{EA}{l},$$

$$k_{12} = -\frac{EA}{l} \text{ and } k_{k+2,k+2} = \left(\frac{k\pi}{l}\sqrt{\frac{E}{\rho}}\right)^2,$$

where ρ is the density; *E* is the Young's modulus; $\omega_k = \frac{k\pi}{l}\sqrt{\frac{E}{\rho}}$ is the *k*th natural frequency. ~

We reported the *multimode vibration* analysis approach to perform heterogeneous data-intensive vibration analysis in complex MEMDs. This concept allows on explicitly integrate complex electromagnetic–mechanical effects and phenomena.

3.3. Vibroacoustics

The sound radiation depends on the structural acceleration, surface geometry, medium, etc. The radiated pressure is found using the Green function *G*, and we have

$$p(t,r,\theta,\phi) = \rho \int_0^{2\pi+R} \int_{-R} \ddot{\omega}(t,\phi,z) G(r,\theta,\phi) d\phi dz.$$

Thus, using the equations derived, one models vibrations and noise in electromechanical motion devices.

IV. Optimal Design For MEMDs

The proposed design paradigm focuses on vibration and noise reduction through optimization of electromagnetic – mechanical – vibroacoustic behavior of MEMDs. Our goal is to minimize vibration, and thus, reduce noise. The major electromagnetic and electromechanical vibroacoustic sources are examined. It was illustrated that the vibration results due to complex direct and indirect electromagnetic, electromechanical and vibroacoustic phenomena, and the optimization of electromagnetic - electromechanical system (*passive vibroacoustic optimization*) and active vibroacoustic control (*active vibroacoustic optimization*) must be performed.

High-fidelity modeling concept was outlined and illustrated in Section 3. The optimal design paradigm is

introduced in this section. The proposed paradigm focuses on vibration and noise reduction through optimization of electromagnetic–mechanical–vibroacoustic behavior. This allows one to minimize vibrations, and thus, reduce the emitted noise. In particular, for MEMDs, the electromagnetic and mechanical systems, as well as vibroacoustic system (interior and exterior geometry, etc.) must be designed and optimized to compensate (attenuate) vibrations. Through optimization of electromagnetic, electromechanical, and vibroacoustic systems, the *passive vibroacoustic optimization* problem can be solved. However, the *passive vibroacoustic optimization*, in general, does not guarantee the desired MEMDs performance. Therefore, the *active vibroacoustic optimization* is under our consideration.

The mathematical formulation of the *active vibroacoustic optimization* problem is given as

$$\min_{\mathbf{u}\in U}\left[\mathbf{r}(t,\mathbf{x}),\ p(t,r,\theta,\phi)\right],$$

where $\mathbf{u}$ is the control vector, $\mathbf{u}\in U$.

Different control variables can be used. For example, for MEMDs that designed as axial and radial topology two-phase permanent-magnet synchronous microelectro-mechanical motion devices [4], the *as* and *bs* phase voltages (u_{as} and u_{bs}) can be considered as the control variables, and $\mathbf{u}=\begin{bmatrix}u_{as} & u_{bs}\end{bmatrix}^T$, $\mathbf{u}\in U$. Due to the control bounds (voltages are limited), we have $\mathbf{u}\in U$. It should be emphasized that stepper micromotors and brushless servomotors have been industrially fabricated using micromachining technology, and the diameter of this micromachines is 2 mm.

In practice, to implement control algorithms, the power amplifiers' duty cycles are controlled by microcontrollers that develop PWM signals. These PWM control signals drive the high-frequency FETs to regulate the voltages. Hence, the electromagnetic field in MEMDs can be controlled in order to attenuate the vibrations and noise. Adaptive reconfigurable controllers are synthesized applying the modern control theory [5]. To implement adaptive control laws, we apply the *information-theoretic* paradigm [5]. It is illustrated that these *premium* control laws can achieve the desired level of intelligence, adaptability and robustness.

The *passive vibroacoustic optimization* can be performed with the ultimate objective to optimize the electromagnetic, electromechanical and vibroacoustic systems. For example, the MEMDs and their components (micromagnets, microwindings, air gap, etc.) geometry can be optimized. In addition to the *passive vibroacoustic optimization*, the *active vibroacoustic optimization* problem has been formulated is examined. Thus, a novel paradigm to attenuate vibrations and noise in MEMDs is reported. The optimal design significantly enhances capabilities and improves performance of MEMDs [4]. Devising and validating the proposed optimization concepts, we radically improve efficiency, robustness and stealth.

The paradigm reported is based upon the optimal electromagnetic–electromechanical design and active vibroacoustic control varying the electromagnetic field. This provides a viable method to attenuate vibrations and reduce noise. Conventional active noise control techniques [2] cannot be applied due to fundamental difficulties. In particular, the major drawbacks are

- it is impossible to measure and attain real-time assessment of the acoustic signals in the full operating envelope;
- it is impossible to set the compensating signal which must be identical in magnitude and be 180 degrees out-of-phase;
- serious hardware limitations, e.g., compensating noise emitting devices cannot be mounded, sensor sensitivity and accuracy, etc.

Compared with the conventional methods, the paradigms reported, is based upon the optimal electromagnetic – mechanical – virboacoustic design, optimization, and active vibration control varying the electromagnetic field. This provides the designer with a viable alternative method to attenuate vibrations and reduce noise in MEMDs and electromechanical motion devices.

V. Experimental Results and Validations

The noise spectra of different axial and radial topology MEMDs were measured and analyzed. In particular, the studied MEMDs are micro- and minimotors fabricated using surface micromachining technology by Maxon, Namiki (2, 10 and 12 mm diameter), Faulhaber (2 mm diameter) and MEMS Fabrication Facilities (0.4 mm diameter). Different variables (radiated noise, vibration, electric field intensity and density, magnetic field intensity and density, electromagnetic torque, current, applied voltage, duty cycle, angular velocity, angular displacement, etc.) are measured and stored to attain data-intensive analysis as well as data acquisition, manipulation and mining. The optimized and computationally efficient MATLAB m-files were developed to perform a coherent analysis. For example, these MATLAB files were used to analyze and visualize signals in the time and frequency domains as well as to perform heterogeneous simulations. The probability and statistical analysis are accomplished utilizing the MATLAB toolboxes as well as complementary files to support the coherent vibroacoustic analysis.

Using the fundamental results reported in section 3, one concludes that due to complex geometrical and structural interfered vibroacoustic systems in MEMDs, the low-, medium- and high-frequency vibrations will result due to short-, middle- and long-wavelength deformations. To attain the *multimode vibration* analysis, the frequency interval must be expanded. For MEMDs, we use the frequency interval from 10 Hz to 20000 Hz.

Comprehensive experimental results for two Namiki minimotors (series 12CL-20N) that operate in different operating envelopes (angular velocity, electromagnetic loads, torque loads, temperature, etc.) were carried out. For different angular velocity, the experimental results are illustrated in Figure 1. It must be observed that MEMDs and minimachines can be driven and controlled using the VLSI-based controller-driver [4] as illustrated in Figure 1.

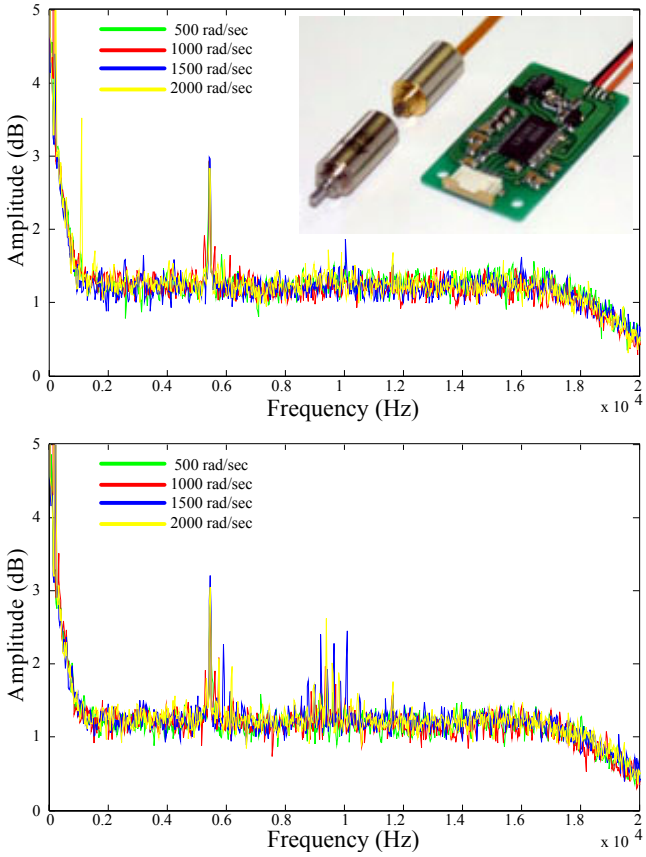

Figure 1. Experimental results for two 12CL Namiki minimotors: noise spectra is reported for different angular velocities

The discrete Fourier transform coefficients for the studied Namiki minimotors (with the noise spectra as reported in Figure 1) are derived. Using the experimental data, Figure 2 illustrates the measured and recovered (synthesized) noise for the examined minimachines for the angular velocity 1500 rad /sec.

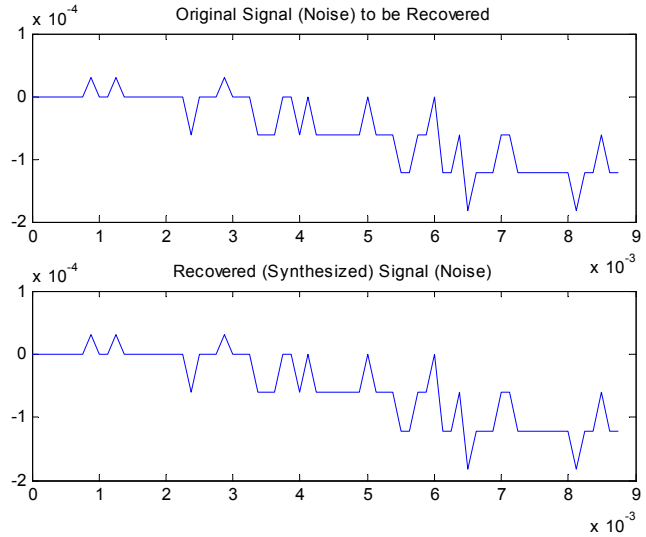

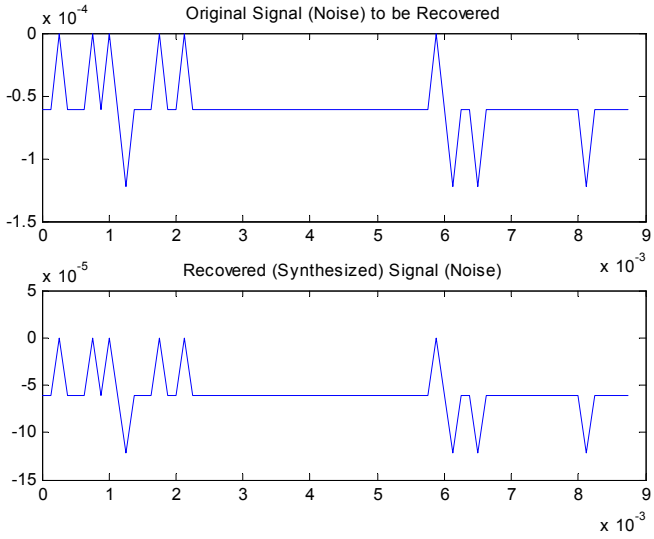

Figure 2. Measured and recovered noise for two minimachines

Other two Namiki minimotors (series 10CL-12) are examined in the rated operating envelope. The experimental results for angular velocities 1000 and 2000 rad/sec are reported in Figure 3.

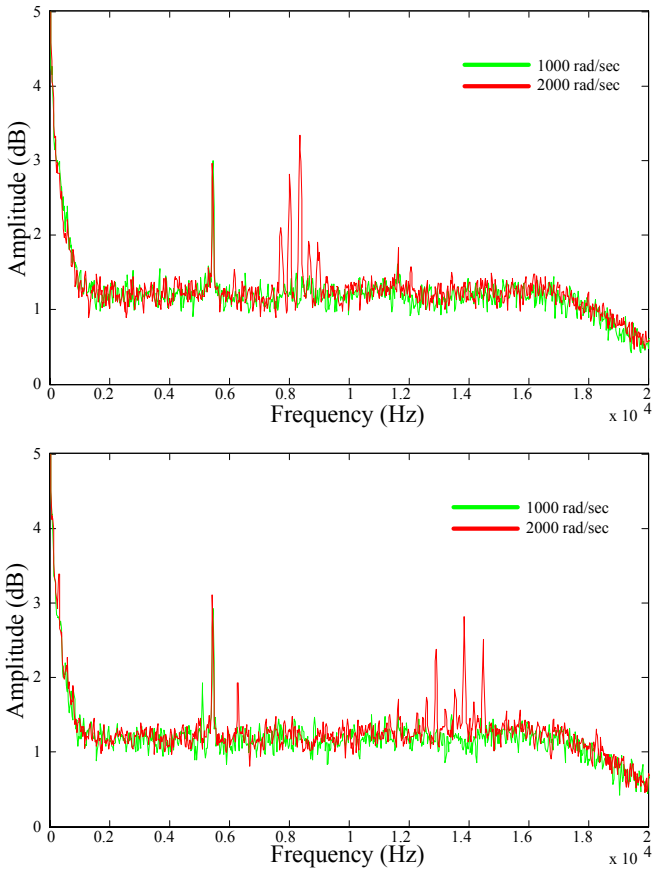

Figure 3. Experimental results for two 10Cl Namiki minimotors: noise spectra for angular velocities 1000 and 2000 rad/sec

It is evident that minimotors exhibit distinct performance, see the experimental results reported in Figures 1 and 3. Furthermore, the vibration and noise significantly vary for different angular velocities and loads. The experimental results documented provide the evidence that only high-fidelity modeling and coherent analysis can provide the desired degree of accuracy in design and optimization. The experiments illustrate that vibration and noise increase with electromagnetic loading due to the lack of an optimal design, high flux densities, electromagnetic loads, magnetic saturation, hysteresis, high-frequency harmonics, and other phenomena.

High-performance MEMDs can be designed utilizing radial and axial topologies [4]. It should be emphasized that it is feasible to fabricate axial topology affordable high-performance MEMDs. One can achieve high torque and power densities utilizing rear-earth micromagnets that can be deposited utilizing the surface micromachining technologies. The most attractive features that the planar windings can be straightforwardly deposited. The fabricated axial topology MEMDs guarantee high angular velocity and electromagnetic torque [4]. Distinct electromagnetic and vibroacoustic characteristics have been observed during the experimental and fundamental studies for radial and axial topologies mini- and micromachines. Figure 4 illustrates the noise spectra for three minimotors that rotate at the angular velocity 300 rad/sec. The conventional radial topology minimotor has higher noise spectra compared with the axial topology minimachine. The stealth minimotor guarantees significant decrease of the vibration and noise as illustrated in Figure 4. In the stealth minimotor, vibration and noise of electromagnetic and mechanical origins were reduced trough the optimal design and control.

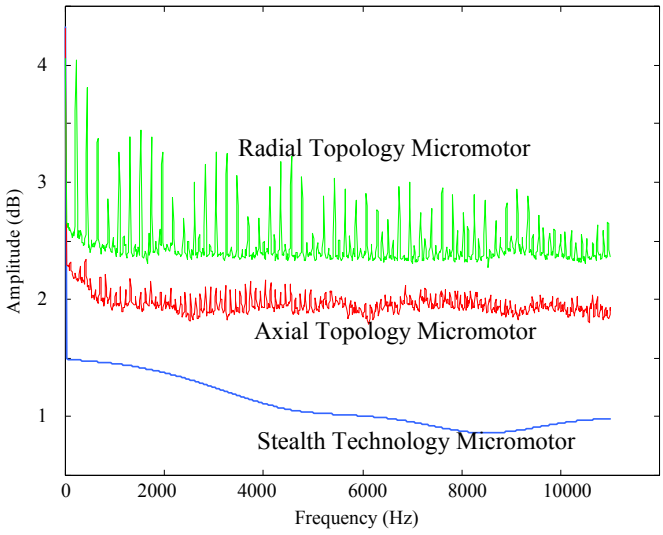

Figure 4. Experimental results for different minimachines

It is found that in the radial topology MEMDs the noise spectra nonlinearly depend upon the operating envelope (electromagnetic field, angular velocity, electromagnetic loads, etc.). For MEMDs the nonlinear phenomena cannot be neglected. Figure 5 documents the noise spectra for an axial minimotor for different angular velocities. The noise peak is observed at 325 rad/sec, and the noise spectra significantly decreased for 300 and 350 rad/sec.

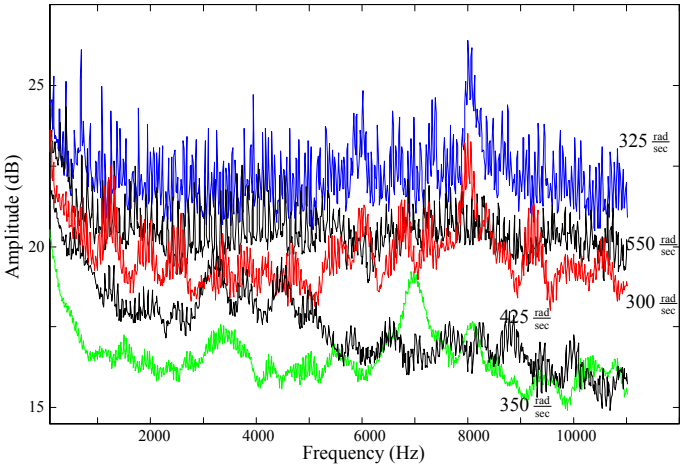

Figure 5. Experimental results: noise spectra for the axial micromotor for five different angular velocities

The experimental, applied and fundamental results reported in this section are new and have not been researched in the literature. In general, the vibroacoustic optimization and stealth at the rated speed and load do not guarantee the desired electromagnetic and vibroacoustic performance in the full operating envelope. Therefore, the entire operating envelope must be studied. We conclude that the coherent electromagnetic, electromechanical and vibroacoustic analysis must be performed using high-fidelity modeling based upon Maxwell's equation, tensor analysis, Lagrangian mechanics, *multimode vibration* analysis concept, as well as vibroacoustic theory. Making use the modeling concept reported in Section 3, nonlinear heterogeneous simulations and data-intensive analysis are performed in the MATLAB environment using the available toolboxes including SIMULINK.

Using the displacement mode equation

$$\mathbf{r}(t,\mathbf{x})=\sum_{k=1}^{\infty}q_{Sk}(t)\phi_{Sk}(\mathbf{x})+\sum_{k=1}^{\infty}q_{Mk}(t)\phi_{Mk}(\mathbf{x})+\sum_{k=1}^{\infty}q_{Lk}(t)\phi_{Lk}(\mathbf{x})$$

for different subsystems (shaft, rotor, shell, shaft, airgap acoustic cavity, bearing, etc.), the bending, torsional and axial elastic waves are examined to analyze the deformations and modes in MEMDs. Having examined vibrations, the radiated pressure $p(t,r,\theta,\phi)$ is found. The radiated pressure is modeled solving the following three-dimensional wave equation

$$\frac{1}{r^2}\frac{\partial}{\partial r}\left(r^2\frac{\partial p}{\partial r}\right)-\frac{1}{c_0^2}\frac{\partial^2 p}{\partial t^2}=0,\ p(t,r)=f_{outwards}(t)+f_{inwards}(t)$$

assuming the spherical symmetry.

To compliment the fundamental results in modeling, simulation and analysis of complex nonlinear electromagnetic–electromechanical–vibroacoustic effects and phenomena, the optimization problem is solved applying the optimal design paradigm reported in Section 4

with the ultimate objective to attain *active vibroacoustic optimization*. The control algorithms, signal processing, signal conditioning and other functions are implemented. It is demonstrated that vibration and noise increase with electromagnetic and torque loads due to the lack of an optimal design, high flux densities, magnetic saturation, hysteresis, high-frequency harmonics, etc. For MEMDs, we apply controlled voltages to the phase windings to attain the superior MEMDs performance. To attain the desired electromagnetic, electromechanical and vibroacoustic systems integrity, there is the need to depart form the conventional active and passive vibration attenuation concepts [2, 3]. We introduce and verify an entirely new paradigm that is based upon the optimization of electromagnetic, mechanical and vibroacoustic systems, vibration reduction and noise attenuation through the optimal electromagnetic-mechanical-vibroacoustic design. In particular, the electromagnetic, mechanical and vibroacoustic systems of motion devices were designed to compensate (attenuate) vibration and noise. In addition to *passive vibroacoustic optimization* (interior/exterior geometry design and optimization), the *active vibroacoustic optimization* problem was researched solving the minimization problem

$$\min_{\mathbf{u}\in U}\left[\mathbf{r}(t,\mathbf{x}),\ p(t,r,\theta,\phi)\right].$$

The basic electromagnetic and electromechanical mechanisms of noise and vibration are reported and studied. It is shown that one can reduce vibration and noise that are due to electromagnetic and mechanical origins. The undesirable components of radial and axial forces (that are due to not optimal design, not perfect fabrication, expanded operating envelope, electromagnetic loads, etc.) largely contribute to the parasitic electromagnetic/electromechanical-origin vibroacoustic. It is shown that these forces can be controlled and minimized. Our major emphases are focused on the development and validation of robust and affordable concepts that guarantee a significant decrease of the vibroacoustic signature, increase efficiency, robustness, reliability, expanded operating envelope, etc. We depart from consideration of vibration and noise in pure mechanical systems because electromagnetic phenomena must be integrated for MEMDs. In addition to basic and applied research, experiments are performed to validate fundamental results. Novel phenomena and effects were observed. The basic theory reported supports and complements the experimental findings.

VI. Conclusions

In this paper, complex electromagnetic, electromechanical and vibroacoustic phenomena in MEMDs were studied. High-fidelity modeling, data-intensive analysis, optimization and experiments were reported. Making use of electromagnetics, mechanics and tensor calculus, we explicitly formulated and solved the integrated electromagnetic – mechanical – vibroacoustic problems from modeling, design and vibration attenuation standpoints. Complex phenomena were described, and novel optimization paradigms to minimize vibroacoustic signature and attain stealth were devised and verified. Complex phenomena and effects were coherently examined. Our results reinforce the need for contemporary integrated nonlinear analysis and optimization. In fact, simplifications and assumptions are not valid. The fundamental, applied, and experimental results reported significantly expand the horizon of the recent developments in the design, analysis, and optimization of high-performance MEMDs. The problems solved are very important to devise novel concepts and design high-performance MEMDs. The reported results lead to maximum efficiency and robustness, noise and vibration reduction, high torque density, etc. In addition to basic research, experiments were performed to validate the fundamental and applied results documented.

We introduce and verify entirely new paradigms that are based upon electromagnetic, electromechanical and vibroacoustic systems optimization and vibration reduction through the optimal design of MEMDs. It is demonstrated that vibration and noise increase with electromagnetic loads. The electromagnetic and electromechanical mechanisms of noise and vibration are reported and studied. It is shown that one can reduce vibration and noise that are due to electromagnetic and mechanical origins. The undesirable components of radial and axial forces (that are due to not optimal design, high flux densities, magnetic saturation, hysteresis, high-frequency harmonics, not ideal shape of micromachined permanent magnets, variation of micromachined MEMDs components geometries, nonuniformity, not perfect windings, elasticity, poor compliance, surface roughness, surface wear, misalignment, etc.) significantly contribute to the parasitic electromagnetic/mechanical-origin vibration and noise. Our major emphases are focused on the development and validation of robust and affordable concepts that guarantee a significant decrease of the vibroacoustic signature, increase of efficiency, robustness, reliability, expanded operating envelope, durability, etc.

References

[1] S. E. Lyshevski, A. G. Singh and M. A. Lyshevski, "High-fidelity modeling, control, and optimization of electromagnetics and vibroacoustics in mini- and micro-scale motion devices and MEMS," *Proceedings of the IASTED International Conference on Intelligent Systems and Control,* pp. 122-125, Clearwater, FL, 2001.

[2] P. A. Nelson and S. J. Elliott, *Active Control of Sound*, Academic Press, London, 1992.

[3] S. J. Yang, *Low-Noise Electrical Motors,* Carendon Press, Oxford, 1981.

[4] S. E. Lyshevski, *MEMS and NEMS: Systems, Devices, and Structures*, CRC Press, Boca Raton, FL, 2002.

[5] S. E. Lyshevski, *Control Systems Theory With Engineering Applications*, Birkh@user, Boston, MA, 2001.